The Astrophysical Journal, 660:L59–L63, 2007 May 1

AEGIS: A PANCHROMATIC STUDY OF IRAC-SELECTED EXTREMELY RED OBJECTS WITH CONFIRMED SPECTROSCOPIC REDSHIFTS

G. Wilson,[1] J.-S. Huang,[2] G. G. Fazio,[2] R. Yan,[3] A. M. Koekemoer,[4] S. Salim,[5] S. M. Faber,[6] J. Lotz,[6] C. N. A. Willmer,[7] M. Davis,[3] A. L. Coil,[7,8] J. A. Newman,[8,9] C. J. Conselice,[10] C. Papovich,[7] M. L. N. Ashby,[2] P. Barmby,[2] S. P. Willner,[2] R. Ivison,[11] S. Miyazaki,[12] and D. Rigopoulou[13]

Received 2006 May 25; accepted 2006 August 15; published 2007 April 6

ABSTRACT

We study 87 extremely red objects (EROs), selected both to have color redder than $R - [3.6] = 4.0$ and to have confirmed spectroscopic redshifts. Together, these two constraints result in this sample populating a fairly narrow redshift range at $0.76 < z < 1.42$. The key new ingredient included here is deep *Spitzer Space Telescope* Infrared Array Camera (IRAC) data. Based on $[3.6] - [8.0]$ color, we demonstrate that it is possible to classify EROs as early-type galaxies, dusty starburst galaxies, or active galactic nuclei (AGNs; power-law types). We present ultraviolet–to–mid-infrared spectral energy distributions (SEDs) and Advanced Camera for Surveys (ACS) images, both of which support our simple IRAC color classification.

Subject headings: galaxies: elliptical and lenticular, cD — galaxies: evolution — galaxies: high-redshift — galaxies: starburst — infrared: galaxies

1. INTRODUCTION

First discovered in the late 1980s (Elston et al. 1988), EROs are defined by their very red optical/near-infrared colors. It has been known for some time that the redness of their color constrains these galaxies to be either early-type galaxies, starburst galaxies reddened by dust, or AGNs (or a combination of these three classes). However, until recently, with observations limited to the *K* band (or shorter wavelengths), it has proven extremely challenging to accurately classify the EROs by type (Mannucci et al. 2002), even in combination with high-resolution *Hubble Space Telescope* imaging (Moustakas et al. 2004).

Although EROs appear to consist of a heterogeneous mix of galaxy classes, the emerging paradigm is that they may well be the high-redshift counterparts and progenitors of local massive E and SO galaxies. Their reliable classification and study, especially at intermediate redshift ($z \sim 1$), can provide crucial constraints on the evolution of massive, starburst, dusty, and/or ultraluminous infrared galaxies (ULIRGs) known to exist at higher redshift, e.g., *BzK* galaxies (Daddi et al. 2004), BX/BM galaxies (Reddy et al. 2005), distant red galaxies (Franx et al. 2003; Papovich et al. 2006; Conselice et al. 2007), and submillimeter and IR-luminous Lyman break galaxies (Huang et al. 2005; Rigopoulou et al. 2006).

In the rest-frame near-IR, old stellar populations show a turndown at wavelengths longer than the rest-frame 1.6 μm "bump," while dusty starburst populations show emission from small hot dust grains. AGN-dominated sources display a power-law SED. In Wilson et al. (2004), we showed how data from *Spitzer* could begin to help us distinguish among different ERO populations. In this Letter, we extend our ERO study to take advantage of the rich panchromatic data set available from the All-Wavelength Extended Groth Strip International Survey (AEGIS). All magnitudes used in this Letter are in AB magnitudes, unless otherwise specified.

2. THE AEGIS DATA SET

The *Spitzer* IRAC (3.6, 4.5, 5.7, and 8.0 μm; Fazio et al. 2004) component of the Extended Groth Strip (EGS) survey spans an area of $120' \times 10'$ (J.-S. Huang et al. 2007, in preparation; see also Huang et al. 2004, 2007 and Barmby et al. 2006). In conducting this ERO study, we also utilized Deep Extragalactic Evolutionary Probe 2 (DEEP2) spectroscopy (M. Davis et al. 2007, in preparation), $u'g'$ imaging (M. L. N. Ashby et al. 2007, in preparation), Canada-France-Hawaii Telescope (CFHT) *BRI* imaging (Coil et al. 2004), ACS *V*(F606W) and *I*(F814W) imaging, deep Subaru *R* (27.0 AB, 5 σ; Miyazaki et al. 2002) and *K* imaging (C. J. Conselice et al. 2007, in preparation), and Multiband Imaging Photometer for *Spitzer* (MIPS; Rieke et al. 2004) 24 μm imaging. Further details may be found in Davis et al. (2007).

3. IRAC-SELECTED GALAXIES AND THEIR COLOR-COLOR DISTRIBUTION

The EGS field contains ~45,000 galaxies detected at 3.6 μm (23.9 AB, 5 σ). Figure 1 shows an $R - [3.6]$ versus $[3.6] - [8.0]$ color-color diagram. The black points show the ~13,000 3.6 μm–selected galaxies with good quality Subaru *R* and 8.0 μm photometry.

The colored tracks in Figure 1 show the location in color-color space as a function of redshift ($0 < z < 4$) for eight nonevolving empirical templates (four common Coleman et al. 1980 [hereafter CWW] templates [E, Sbc, Scd, Im] empirically extended to 10 μm using *Infrared Space Observatory* data

[1] *Spitzer* Science Center, California Institute of Technology, Pasadena, CA 91125; gillian@ipac.caltech.edu.
[2] Harvard-Smithsonian Center for Astrophysics, Cambridge, MA 02138.
[3] Department of Astronomy, University of California, Berkeley, CA 94720.
[4] Space Telescope Science Institute, Baltimore, MD 21218.
[5] Department of Physics and Astronomy, University of California, Los Angeles, CA 90095.
[6] UCO/Lick Observatory and Department of Astronomy and Astrophysics, University of California, Santa Cruz, CA 95064.
[7] Steward Observatory, University of Arizona, Tucson, AZ 85721.
[8] Hubble Fellow.
[9] Institute for Nuclear and Particle Astrophysics, Lawrence Berkeley National Laboratory, Berkeley, CA 94700.
[10] School of Physics and Astronomy, University of Nottingham, Nottingham NG7 2RD, UK.
[11] Astronomy Technology Centre, Royal Observatory, Edinburgh EH9 3HJ, UK.
[12] Subaru Telescope, National Astronomical Observatory of Japan, Hilo, HI 96720.
[13] Department of Astrophysics, Oxford University, Oxford OX1 3RH, UK.

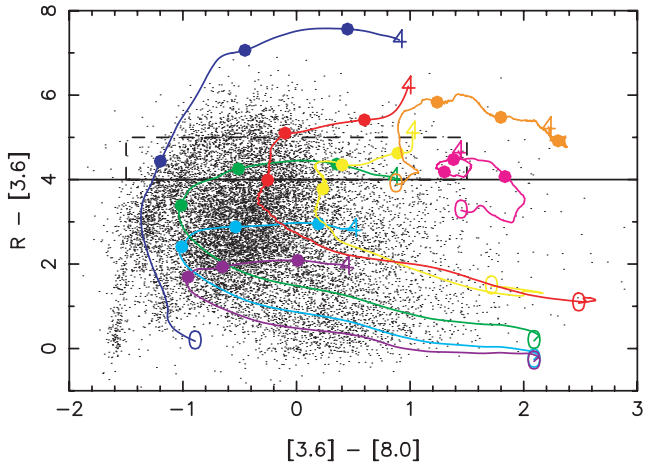

FIG. 1.—$R - [3.6]$ vs. $[3.6] - [8.0]$ color-color diagram for IRAC-selected galaxies. The solid lines show nonevolving templates in color-color space for CWW early-type (*blue*), CWW Sbc (*green*), CWW Scd (*cyan*), CWW Im (*purple*), dusty starburst M82 (*red*), dusty starburst/ULIRG Arp 220 (*yellow*), NGC 1068 (*pink*), and NGC 5506 (*orange*). The redshift is indicated for each type. A distinctive swath of galaxies is apparent curving from the left to the top of the figure. The CWW early-type (*blue*) track follows this extremely well to $z \sim 0.7$, when the template noticeably begins to diverge from the "bluer" data. The plume in the lower left-hand corner is caused by stellar contamination. Galaxies with $R - [3.6] > 4.0$ (i.e., above the black line) are defined as EROs. One would expect only high-redshift ($z > 0.8$) early-type galaxies, ($z > 1.0$) dusty starburst galaxies, ($z > 1.5$) CWW Sbc galaxies, and AGNs (at any redshift) to satisfy this extremely red criterion. The dashed black rectangle indicates the region of color-color space populated by the 87 EROs with confirmed spectroscopic redshifts (see also the bottom panel of Fig. 2 and § 5).

[J.-S. Huang et al. 2007, in preparation], a dusty starburst template [M82], a dusty starburst/ULIRG template [Arp 220], and two AGN templates [NGC 1068 and NGC 5506]). While we fully expect these templates to become increasingly inaccurate at high redshift, they do serve to provide us with a simple insight into the likely nature and redshift distribution of galaxies within this color-color diagram.

A distinctive swath of galaxies is clearly apparent curving from the left to the top of Figure 1 (the plume in the lower left-hand corner is caused by stellar contamination). Notice, especially, the excellent agreement between this swath of galaxies observed in color-color space and the CWW E (*blue*) track to $z \sim 0.7$, when the template noticeably begins to diverge from the "bluer" data. We note that the predictability of the $[R] - [3.6]$ color-redshift relation for early-type galaxies can be utilized as an effective technique for detecting high-redshift clusters of galaxies, e.g., at $z < 1.4$ in the 4 deg^2 *Spitzer* First Look Survey field (Wilson et al. 2005; A. Muzzin et al. 2007, in preparation). The SpARCS collaboration[14] is currently utilizing an even redder $[z'] - [3.6]$ color to detect and study clusters to $z = 2$ in the 50 deg^2 *Spitzer* SWIRE Legacy fields (Wilson et al. 2006).

We *define* an ERO to be a galaxy redder in color than $R - [3.6] = 4.0$. This is the same criterion used in Wilson et al. (2004) and is a very similar selection criterion to the traditional Vega $R - K > 5.0$ requirement (see Wilson et al. 2004 for a discussion).

From Figure 1, we might expect that only high-redshift galaxies ($z \gtrsim 0.8$), early-type galaxies ($z \gtrsim 1.0$), dusty starburst galaxies, and AGNs (at any redshift) would satisfy this extremely red criterion. As we shall demonstrate in the remainder of this Letter, this indeed turns out to be the case. Note that

[14] See http://spider.ipac.caltech.edu/staff/gillian/SpARCS.

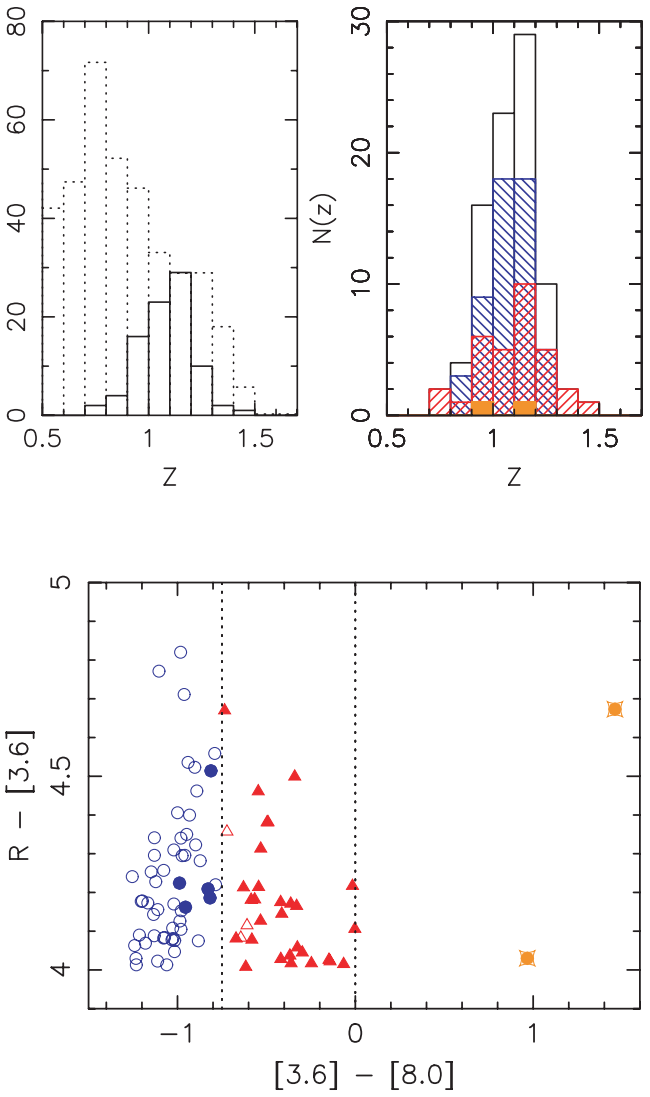

FIG. 2.—The solid black histogram in the top left panel shows the ERO redshift distribution $N(z)$ (which peaks for this sample of 87 EROs at $z = 1.15$). The dotted black histogram illustrates the underlying DEEP2 selection function in the EGS field *before* the ERO criterion is applied. It also shows the redshift distribution $N(z)$ of all 6023 galaxies with good quality redshift determinations, scaled down by a factor of 15 for comparison with the ERO $N(z)$. The bottom panel (dashed black rectangle in Fig. 1) shows our IRAC $[3.6] - [8.0]$ color division into early-type (*blue circles*), dusty starburst (*red triangles*), and power-law (*orange squares*) EROs. The filled symbols indicate the 36 EROs with a 24 μm detection (19.1 AB, 5 σ, § 7). Also shown in the top right panel (and discussed in § 5) is the redshift distribution of the full sample (*solid black histogram*) and the three subclasses (using the same blue, red, and orange color scheme).

late-type CWW Scd (*cyan*) and irregular (*purple*) galaxies are *never* sufficiently red to be classified as an ERO *at any redshift*, and one would not expect to find any CWW late-type Sbc (*green*) EROs at $z < 1.5$.

4. REDSHIFT DISTRIBUTION OF THE SPECTROSCOPIC ERO SAMPLE

There are several thousand EROs in the EGS field. Here we carry out a pilot study of the 87 EROs with confirmed DEEP2 spectroscopic redshifts. We use spectroscopy in this Letter only for redshift determination.

The solid black histogram in the top left panel of Figure 2 shows the redshift distribution of the 87 EROs in our sample.

The EROs occupy a relatively narrow redshift range at $0.76 < z < 1.42$. The dotted black histogram shows the redshift distribution of those galaxies in the DEEP2 EGS field with good quality spectroscopic redshift determinations (scaled down by a factor of 15).

The fact that none of the EROs are located at $z < 0.76$ is not a DEEP2 selection effect; in EGS, DEEP2 samples the full redshift range $0 < z < 1.45$ (Faber et al. 2005; Willmer et al. 2006). It is caused by the additional ERO $R - [3.6] > 4.0$ selection requirement, which effectively excludes low-redshift galaxies (Fig. 1). The DEEP2+ERO selection function also limits this sample to a fairly bright but narrow range of $18.5 < [3.6] < 20$, with the one exception of 12007954, a 17th magnitude AGN (Le Floc'h et al. 2007). Note that by selecting only those EROs with spectroscopic redshifts, we may bias our sample against inclusion of any low-redshift, extremely dusty galaxies (since optically faint galaxies will not pass the $R < 24.1$ selection requirement of the DEEP2 survey).

5. ERO CLASSIFICATION USING [3.6] − [8.0] COLOR

It is possible to divide the EROs in this sample into three broad classes by means of their IRAC [3.6] − [8.0] color. In this section, we introduce each of these classes, show examples of their SEDs, and discuss the occasionally subtle features that are only apparent from such broad-baseline data sets. We also study their morphologies using ACS images.

From Figure 1, early-type galaxies are expected to have the bluest ($[3.6] - [8.0] \simeq -1.0$) colors, dusty starburst galaxies are expected to have intermediate colors ($[3.6] - [8.0] \simeq -0.5$), and AGNs are expected to have the reddest colors ($[3.6] - [8.0] \simeq +1.0$). The bottom panel of Figure 2 corresponds to the dashed rectangle in Figure 1 and shows the subsample of 87 EROs with spectroscopic redshifts. We *classify* $[3.6] - [8.0] < -0.75$ galaxies as bulge-dominated early types (*blue circles*), $-0.75 < [3.6] - [8.0] < 0.0$ galaxies as dusty starburst types[15] (*red triangles*), and $[3.6] - [8.0] > 0.0$ galaxies as power-law AGN types (*orange squares*). As we shall demonstrate, these two simple color cuts do separate the classes rather well. This is because the redshift distribution of this particular sample is rather narrow. For a sample spanning a broader redshift distribution, one might imagine utilizing a more complex color selection to isolate the meanderings of the different populations through color-color space in Figure 1.

We classify 53 of the EROs as early-type galaxies. They are located at $0.82 < z < 1.28$, and their redshift distribution is shown by the blue hatching in the top right panel of Figure 2. We classify 32 EROs as being dusty starburst types. The dusty starburst population (shown by the red hatching) has a slightly wider redshift distribution from $0.76 < z < 1.42$ (presumably because galaxies in this class can contain arbitrary amounts of dust). We classify two EROs as being predominantly power-law types. These are 12007878 at $z = 0.99$ and 12007954 at $z = 1.15$, and they are shown in solid orange (see also Konidaris et al. 2007).

6. EXAMPLE SEDs AND ACS IMAGES

The top and bottom panels of Figure 3 (Plate 1) show examples of observed SEDs and $3'' \times 3''$ *I*-band (F814W) postage-stamp ACS images. For comparison, we also show the CWW E (*blue curve*) and M82 (*red curve*) templates (§ 3) as they would appear at the redshift of each ERO. At $z \sim 1$, IRAC's 8 μm channel measures any emission from small hot dust grains (indicative of a dusty starburst galaxy), while the 3.6 μm channel measures the stellar peak. Therefore, a relative red (or blue) [3.6] − [8.0] color can be used to discriminate for (or against) dusty starburst galaxies (and AGNs) at this redshift.

6.1. *Early-Type EROs*

The top panel of Figure 3 shows six examples of galaxies that are color-classified (using IRAC) as early-type EROs. The CWW E template approximates the 13048898, 13019047, 13004276, and 12004426 SEDs very well. The CWW E template appears to underestimate the SEDs of 13019309 and 12008091 in the UV. In all cases, the ACS images show clear evidence of bulge-dominated morphologies, supporting our color classification as early-type galaxies.

A total of 35 of the 53 early-type EROs fall within the ACS footprint. A close inspection of all of the available ACS images reveals them to be predominantly bulge-dominated (E-, S0-, or Sa-type spirals). A small number (~10%) appear to be undergoing mergers. We conclude that choosing a blue [3.6] − [8.0] color successfully selects for $z = 1$ EROs with old stellar populations and against those with dusty starburst or power-law features.

6.2. *Dusty Starburst and Power-Law EROs*

The bottom panel of Figure 3 shows five examples of galaxies color-classified (using IRAC) as dusty starburst EROs and one example of a galaxy color-classfied as a power-law ERO (12007878). The M82 template approximates the SEDs of sources 13042940, 12100899, and 12007831 very well, and that of 13004291 reasonably well. In addition to being more mid-IR luminous than an early-type ERO of similar 3.6 μm magnitude, the SEDs of these four sources are more luminous in the optical. Their ACS images show clear evidence of disturbed, peculiar, interacting, or merging galaxies.

Neither template approximates well the SED of 12008048. Close inspection of the ACS image reveals it to be a face-on spiral galaxy. Since a normal spiral at $z = 0.9$ would not meet the $R - [3.6]$ redness criterion, we infer that 12008048 must be an especially dusty spiral.

A total of 17 of the 32 EROs that we classify as dusty starbursts fall within the ACS footprint. Close inspection of all of their images reveals many of them (~60%) to be disturbed or interacting galaxies, and the remainder (~40%) to be late-type spirals.

12007878 shows a monotonically increasing power-law SED. Its host galaxy is clearly bulge-dominated, and it can be unequivocally classified as an AGN-dominated source.

7. DISCUSSION

Turning to those EROs that have 24 μm detections, there are five ($17.4 < [24] < 19.1$) among the 53 early-type EROs and 29 ($16.8 < [24] < 19.1$) among the 32 dusty starburst EROs. Both power-law EROs have a 24 μm detection (14.5 and 16.5). In four out of the five cases of early-type EROs with a 24 μm detection, an ACS image is available. In all four cases, a merging galaxy with several close neighbors is apparent. The MIPS point-spread function is 6″, so it is possible that the signal in each case might be associated with another galaxy entirely.

We use Figure 7 in Le Floc'h et al. (2005) to translate our

[15] We use the word "starburst" to mean a galaxy whose IR luminosity is powered by star formation. We do not intend to imply that these galaxies have total IR luminosity $L(8\text{–}1000\ \mu\text{m}) < 10^{11}\ L_{\odot}$. Indeed, as we shall discuss in § 7, most of these dusty starburst EROs would actually be classified as LIRGs.

24 μm flux limit (80 μJy, 19.1 AB, 5 σ) into a lower limit on the total detectable IR luminosity of an ERO in our redshift range. Depending on the model used, at $z \sim 0.75$, we are capable of detecting sources more luminous than $\sim 5 \times 10^{10}\ L_{\odot}$, i.e., some dusty starbursts, and all LIRGs and ULIRGs. At $z \sim 1.4$, we are capable of detecting sources more luminous than $\sim 5 \times 10^{11}\ L_{\odot}$, i.e., LIRGs and ULIRGs. Based on their actual 24 μm magnitudes and redshifts, most of our "starburst" sources have intrinsic luminosities between 10^{11} and $10^{12}\ L_{\odot}$, i.e., LIRG class. Both of the "AGN" sources have intrinsic luminosities of $>10^{12}\ L_{\odot}$, putting them in the ULIRG class.

Although, in this study, we utilized optical/IRAC colors to classify our ERO sample, IRAC − [24] color selection may be a more effective discriminator at higher redshift (Lacy et al. 2004; Ivison et al. 2004; Sajina et al. 2005).

Putting IRAC ERO colors in the context of perhaps more familiar rest-frame optical colors, Figure 4 shows *rest-frame* $U - B$ color versus *observed* [3.6] − [8.0] color for all IRAC-detected galaxies with good [8.0] and good CFHT *BRI* photometry (see Willmer et al. 2006 for details of the conversion to rest-frame $U - B$). The symbols are the same as in Figure 2. The filled circles in Figure 4 denote the 36 EROs that are also detected at 24 μm (see also Fig. 2). The EROs that we classify as early-type galaxies generally tend to lie on the $U - B$ defined "red sequence," and the EROs that we classify as dusty starburst galaxies tend to lie in the "green valley" and at the top of the "blue cloud" (Weiner et al. 2005).

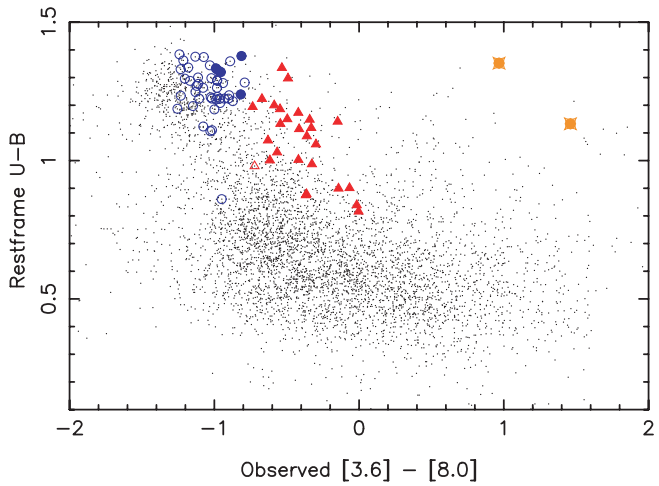

FIG. 4.—Rest-frame $U - B$ color vs. observed [3.6] − [8.0] color for all IRAC-detected galaxies with good [8.0] *and* good CFHT *BRI* photometry. Note that $(U - B)_{\rm Vega} = (U - B)_{\rm AB} - 0.85$. The blue circles indicate bulge-dominated early-type EROs. The red triangles indicate dusty starburst EROs. The orange squares indicate the two AGNs. The filled symbols indicate a 24 μm detection. Is it possible that the 24 μm detections associated with each of the early-type EROs may be spurious and may actually be associated with a close neighbor galaxy (see § 7)? The early-type EROs generally tend to lie on the $U - B$ defined red sequence, and the dusty starburst EROs tend to lie in the "green valley" and at the top of the "blue cloud."

8. CONCLUSIONS

In this Letter, we utilized the AEGIS data set to explore the nature of 87 EROs with confirmed spectroscopic redshifts. IRAC imaging facilitated dividing this sample into three distinct classes using a simple [3.6] − [8.0] color selection technique. We presented SEDs and high-resolution ACS images supporting our (early-type, dusty starburst, or power-law) classification.

We showed that the three classes of EROs and their redshift distribution were broadly consistent with what one would expect from a simple color-color diagram (Fig. 1). We found 53 early-type galaxies, 32 dusty starburst galaxies/LIRGs, and two obvious AGNs. Both of these AGNs would be classified as ULIRGs.

The selection of this particular sample of EROs was subject to the spectroscopic biases discussed in § 4. We next plan to extend this study to the several thousand IRAC-selected EROs in the AEGIS *without* spectroscopic redshifts.

This work is based in part on observations made with the *Spitzer Space Telescope*, which is operated by the Jet Propulsion Laboratory, California Institute of Technology, under a contract with NASA. Support for this work was provided by NASA through an award issued by JPL/Caltech. A. L. C. is supported by NASA through Hubble Fellowship grant HF-01182.01-A. We thank the referee, Matt Malkan, for constructive comments. G. W. thanks Mark Lacy, Adam Muzzin, Jason Surace, Ian Smail, and Mike Hudson for useful discussions, and UC Berkeley and UC Santa Cruz for their hospitality.

REFERENCES

Barmby, P., et al. 2006, ApJ, 642, 126
Coil, A. L., Newman, J. A., Kaiser, N., Davis, M., Ma, C.-P., Kocevski, D. D., & Koo, D. C. 2004, ApJ, 617, 765
Coleman, G. D., Wu, C.-C., & Weedman, D. W. 1980, ApJS, 43, 393 (CWW)
Conselice, C. J., et al. 2007, ApJ, 660, L55
Daddi, E., Cimatti, A., Renzini, A., Fontana, A., Mignoli, M., Pozzetti, L., Tozzi, P., & Zamorani, G. 2004, ApJ, 617, 746
Davis, M., et al. 2007, 660, L1
Elston, R., Rieke, G. H., & Rieke, M. J. 1988, ApJ, 331, L77
Faber, S. M., et al. 2005, preprint (astro-ph/0506044)
Fazio, G. G., et al. 2004, ApJS, 154, 10
Franx, M., et al. 2003, ApJ, 587, L79
Huang, J.-S., et al. 2004, ApJS, 154, 44
———. 2005, ApJ, 634, 137
———. 2007, 660, L69
Ivison, R. J., et al. 2004, ApJS, 154, 124
Konidaris, N., et al. 2007, ApJ, 660, L7
Lacy, M., et al. 2004, ApJS, 154, 166
Le Floc'h, E., et al. 2005, ApJ, 632, 169
———. 2007, ApJ, 660, L65
Mannucci, F., Pozzetti, L., Thompson, D., Oliva, E., Baffa, C., Comoretto, G., Gennari, S., & Lisi, F. 2002, MNRAS, 329, L57
Miyazaki, S., et al. 2002, PASJ, 54, 833
Moustakas, L. A., et al. 2004, ApJ, 600, L131
Papovich, C., et al. 2006, ApJ, 640, 92
Reddy, N. A., Erb, D. K., Steidel, C. C., Shapley, A. E., Adelberger, K. L., & Pettini, M. 2005, ApJ, 633, 748
Rieke, G. H., et al. 2004, ApJS, 154, 25
Rigopoulou, D., et al. 2006, ApJ, 648, 81
Sajina, A., Lacy, M., & Scott, D. 2005, ApJ, 621, 256
Weiner, B. J., et al. 2005, ApJ, 620, 595
Willmer, C. N. A., et al. 2006, ApJ, 647, 853
Wilson, G., et al. 2004, ApJS, 154, 107
———. 2005, preprint (astro-ph/0503638)
———. 2006, preprint (astro-ph/0604289)

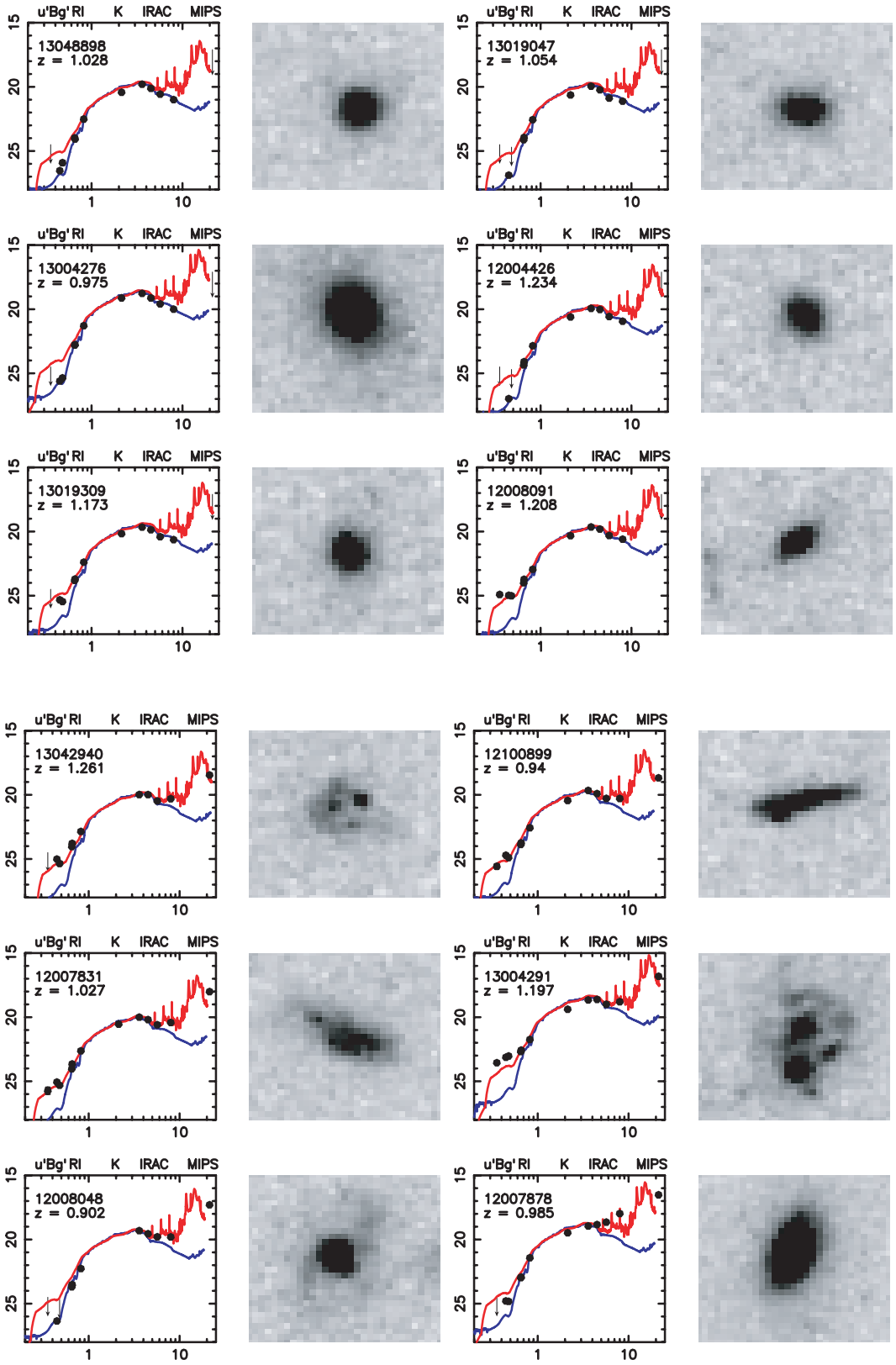

PLATE 1

FIG. 3.—*Top*: Examples of observed SEDs (*left*) and 3″ × 3″ *I*-band ACS images (*right*) for six IRAC color-selected early-type EROs. A maximum of 12 passbands (u', *B*, g', Subaru *R*, CFHT *R*, *I*, and *K*, and [3.6], [4.5] [5.8], [8.0], and [24.0]) are shown. The tip of the downward-pointing arrow indicates upper limits in the case of nondetections. Each panel shows the DEEP2 ID number and the spectroscopic redshift. Also shown are CWW E (*blue curve*) and M82 (*red curve*) templates (§ 3) as they would appear at the redshift of each ERO. See § 6 for discussion. *Bottom*: Same as the top panel, but for five IRAC color-selected dusty starburst EROs and one power-law ERO (12007878). The M82 dusty starburst template approximates the 13042940, 12100899, and 12007831 SEDs very well, and that of 13004291 reasonably well. In most cases, the ACS images show clear evidence of interactions and mergers. 12008048 is a face-on dusty spiral galaxy.